J Mater Sci (2009) 44:4264–4269
DOI 10.1007/s10853-009-3620-7

Tensile deformation of a Mg–2.54Nd–0.26Zn–0.32Zr alloy at elevated temperature

Z. L. Ning · G. J. Wang · F. Y. Cao · J. F. Sun · J. F. Du

Received: 3 March 2009 / Accepted: 18 May 2009 / Published online: 5 June 2009

Abstract The engineering stress versus engineering strain curves for a Mg–2.54Nd–0.26Zn–0.32Zr cast alloy were measured by Gleeble-1500D thermo-simulation machine in the temperature range of room temperature to 400 °C at initial strain rates of 10^{-4}–10^{-2} s^{-1}. The effects of strain rate on stress, elongation to facture, and section shrinkage were analyzed. The fractograph morphologies were investigated by using SEM. It was found that strain rate has little effect on engineering stress for the Mg–2.54Nd–0.26Zn–0.32Zr alloy when tested at below 250 °C. When tested at above 250 °C, low strain rate resulted in decreased engineering stress, increased elongation to fracture, and section shrinkage. The fracture mode is cleavage fracture with elongated dimple below 250 °C and changes to typical ductile failure when tested above 250 °C.

Introduction

Magnesium alloys are considered as potential candidates for many structural application due to their low density and excellent castability and machinability [1–4]. Mg–RE–Zr alloys, as a group of speciality light alloys, have found important applications in aerospace, military, automotive, and other industries, both as wrought and sand or permanent mold cast alloys [5, 6]. Currently the Mg–RE–Zr system is the only magnesium alloy system that can offer adequate creep resistance for application at temperature above 200 °C [7]. Mg–Nd–Zn–Zr alloys, one of two major Mg alloy systems have proven to be suitable for operating at 250 °C. The other is yttrium and rare earth containing WE series Mg alloy system [1, 2, 8]. Both types of alloys are sand casting alloys. At the fully grain-refined state, the microstructure of a Mg–Nd–Zn–Zr alloy is such that a hard $Mg_{12}Nd$ or $Mg_{12}(Nd,Zn)$ intermetallic phase exists at both triple points and along the grain boundaries, acting to lock the grain boundaries and reduce grain boundary and dislocation sliding [9, 10]. Compared with WE series Mg alloy system, Mg–Nd–Zn–Zr alloys are much cheaper and demonstrate more attractive cost-effectiveness. Understanding the tensile deformation behaviors and fracture mechanism of Mg–Nd–Zn–Zr alloys at elevated temperature is of great engineering interest.

The present study aims at the tensile properties and fracture mechanism of a Mg–Nd–Zn–Zr alloy up to 400 °C.

Experimental procedure

The 99.9% Mg, 99.9% Zn, Mg-30%Nd master, and Mg-33.3%Zr master were used as raw materials in this investigation. Alloys were prepared in a BN-coated mild steel crucible in an electrical resistance furnace. RJ2 cover flux (main compositions: 38–46% $MgCl_2$, 32–40% KCl, 5–8% BaCl, 3–5% CaF_2, and 8% NaCl + CaCl) and Ar gas were used as a mixed protection and RJ5 flux (main compositions: 24–30% $MgCl_2$, 20–26% KCl, 28–31% $BaCl_2$, 13–15%CaF_2, and 8% NaCl + CaCl) was used as refining agent. The melt was poured into a sand mold with

Z. L. Ning (✉) · F. Y. Cao · J. F. Sun · J. F. Du
School of Materials Science and Engineering, Harbin Institute of Technology, Harbin 150001, China
e-mail: zhiliangning@sina.com

G. J. Wang
Northeast Light Alloy Co., Ltd, Harbin 150060, China

a cylindrical cavity of 30 mm in diameter and 70 mm in depth. The composition was measured by ICPS as 2.54% Nd, 0.26% Zn, 0.32% Zr (soluble Zr), and Mg balance. Alloys were solution treated at 545 ± 5 °C for 12 h, followed by aging at 205 ± 5 °C for 12 h. The microstructure of the heat treated Mg–2.54Nd–0.26Zn–0.32Zr alloy consists of α-Mg matrix and $Mg_{12}Nd$ intermetallic phase uniformly distributed on the matrix as crossed plate by spotted state phase with grain size of 82 μm [9]. Tensile specimens with gauge diameter of Φ5 mm were machined from the heat-treated ingot. The tensile tests at elevated temperature were carried out on Gleeble-1500D Instron electronic universal materials testing machine. The temperatures tested were 100 °C, 200 °C, 250 °C, 300 °C, and 400 °C; and the initial strain rates were set to be 10^{-2} s^{-1}, 10^{-3} s^{-1}, and 10^{-4} s^{-1}, respectively. The heating time and dwelling time prior to tensile tests were all 5 min to ensure temperature uniformity. The test chamber was vacuumed to 0.6 Pa to minimize the oxidation of specimens at test temperatures above 200 °C. The fractured surface was observed in a FEI Sirion scanning electron microscope.

Results and discussions

Engineering stress versus engineering strain

The typical engineering stress versus engineering strain curves are shown in Fig. 1a–e. Strain rate has little effect on the engineering stress at test temperatures of 100 °C and 200 °C. The engineering stress increased sharply with increased engineering strain to reach a peak, followed by a relatively slow increase until fracture. At 250 °C, the midst strain rate of 10^{-3} s^{-1} led to a maximum engineering stress compared with the other two strains rate of 10^{-4} s^{-1} and 10^{-2} s^{-1}. The experiments were repeated three times and the results were the same. At test temperature of 300 °C, the engineering stress quickly reaches a peak at a very

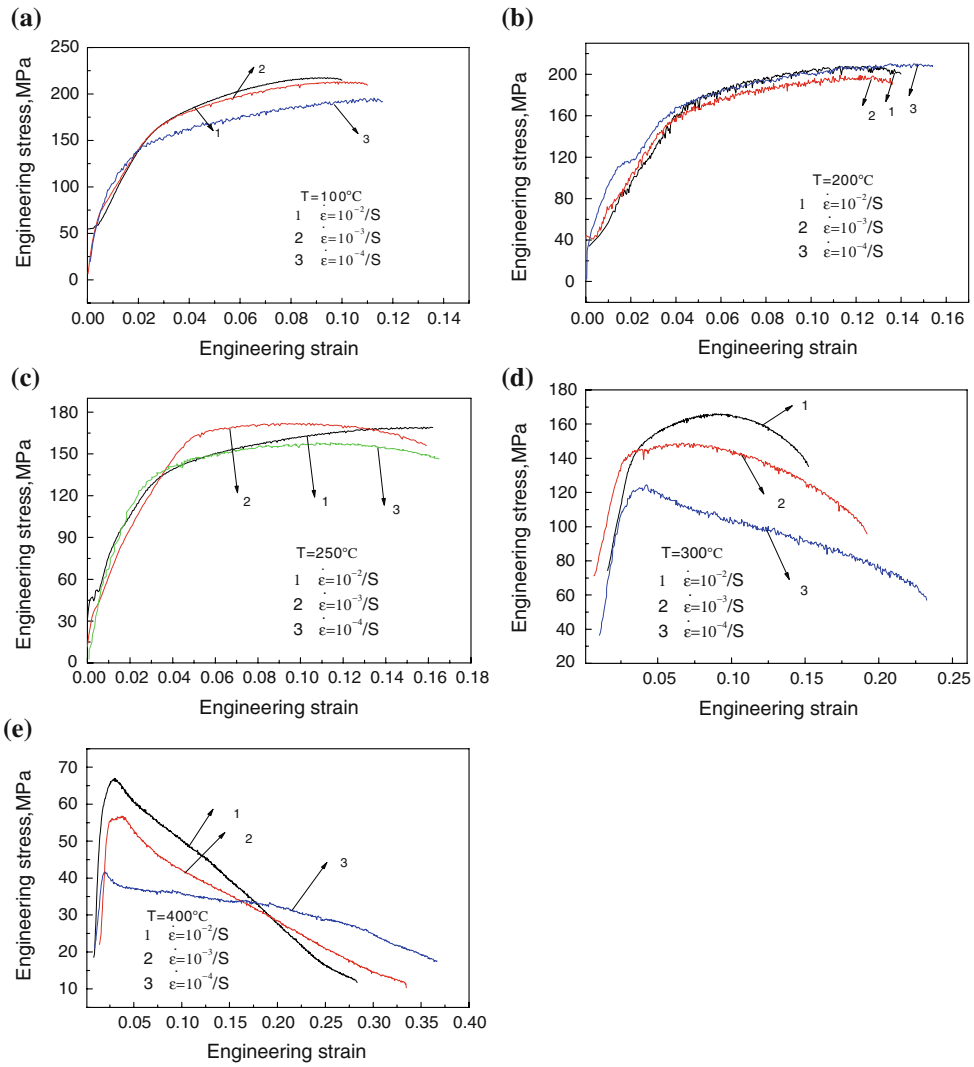

Fig. 1 Engineering stress versus engineering strain curves. **a** 100 °C, **b** 200 °C, **c** 250 °C, **d** 300 °C, and **e** 400 °C

small engineering strain, followed by a slight increase to the maximum and decrease subsequently until fracture at the relatively high strain rates of 10^{-2} s^{-1} and 10^{-3} s^{-1}. For the lowest strain rate of 10^{-4} s^{-1}, the engineering stress reached the maximum sharply, and followed by a linear decrease with engineering strain increasing until fracture. When the test temperature was increased to 400 °C, the engineering stress change was similar with those when tested at 300 °C at the lowest strain rate used in this study. High strain rate resulted in a sharper decrease in engineering stress after it reached the maximum value. Three engineering stress curves intersected at an approximate engineering strain of 0.18. The yield strength and ultimate strength against test temperature are shown in Fig. 2. The elongation to fracture and section shrinkage as a function of test temperature are shown in Fig. 3, demonstrating that they increase significantly when the test temperature is above 250 °C. Lower strain rate results in an increase in elongation to fracture, but has little effect on section shrinkage.

For convenient analysis, a parameter, λ, defined as $\lambda = d\sigma/d\varepsilon$ was used, where σ is engineering stress and ε engineering strain. It is the slope of engineering stress versus engineering strain curve, and corresponds the change tendency of stress fundamentally. Figure 4 represents four typical λ curves. When tested at low temperatures of 100 °C and 200 °C, the engineering stress increases with increased engineering strain until fracture takes place at a low engineering strain of 0.12–0.15. The severe work-hardening results in tensile stress reaching the tensile strength very quickly. Figure 4a shows that the parameter λ decreases gradually during tensile deformation. At initial deformation stage, the density of dislocation enhances incessantly and the homogeneous dislocations stack and entangle each other, leading to an increase in the tensile stress sharply. When this reaches some degree, heterogeneous dislocations encounter and climb takes place for some dislocations, leading to a slight decrease in engineering stress. Only at the maximum strain the negative λ appears, which can be neglected. This suggests that no necking takes place and the fracture mode is brittle. Compared with that at 100 °C, the λ appears to be negative at the late deformation stage tested at 250 °C with medium strain rate used as shown in Fig. 4b, indicating that there exists an obvious necking before fracture takes place. This is in agreement with the macroscopic observation of the fractured specimens. The λ tested at 300 °C with strain rate of 10^{-2} s^{-1} is similar with that at 250 °C with strain rate of 10^{-4} s^{-1}. Comparison between Fig. 4b and c indicates that the latter has a relatively large value, suggesting its stress decrease tendency is faster than the former. Changes of λ values at 400 °C are similar with those tested at 300 °C with strain rates of 10^{-3} s^{-1} and 10^{-4} s^{-1} basically. There are apparent engineering stress peaks existing followed by sharp decrease, showing that necking takes place once the peak reaches until fracture with a large deformation. The λ

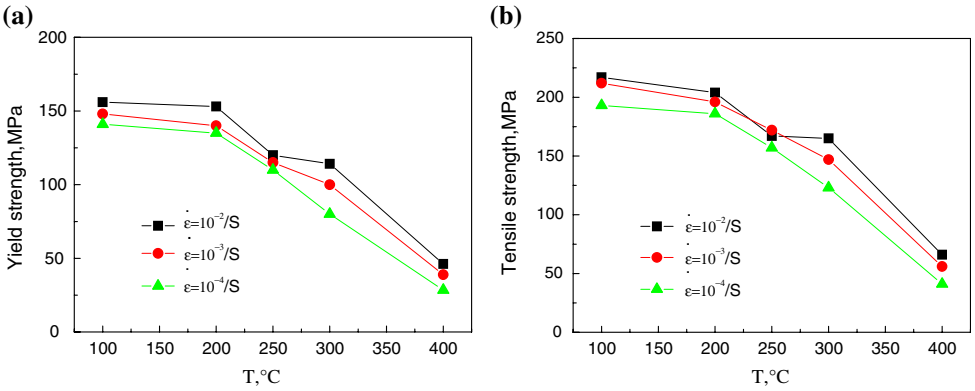

Fig. 2 The yield strength and tensile strength as a function of testing temperature: **a** yield strength and **b** tensile strength

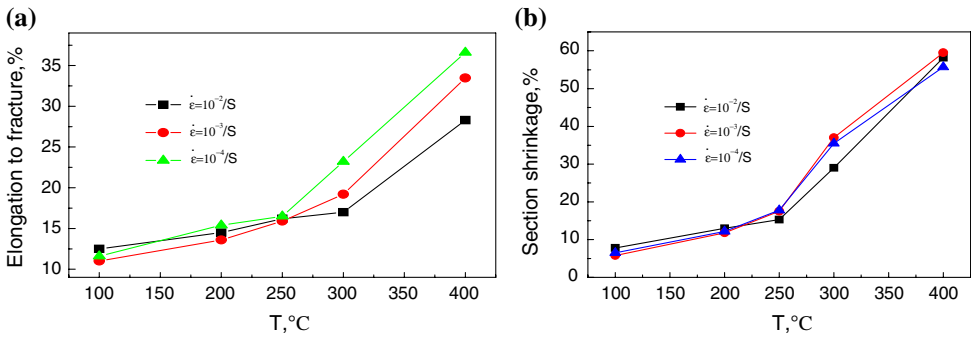

Fig. 3 The elongation and section shrinkage as a function of temperature tested: **a** elongation and **b** section shrinkage

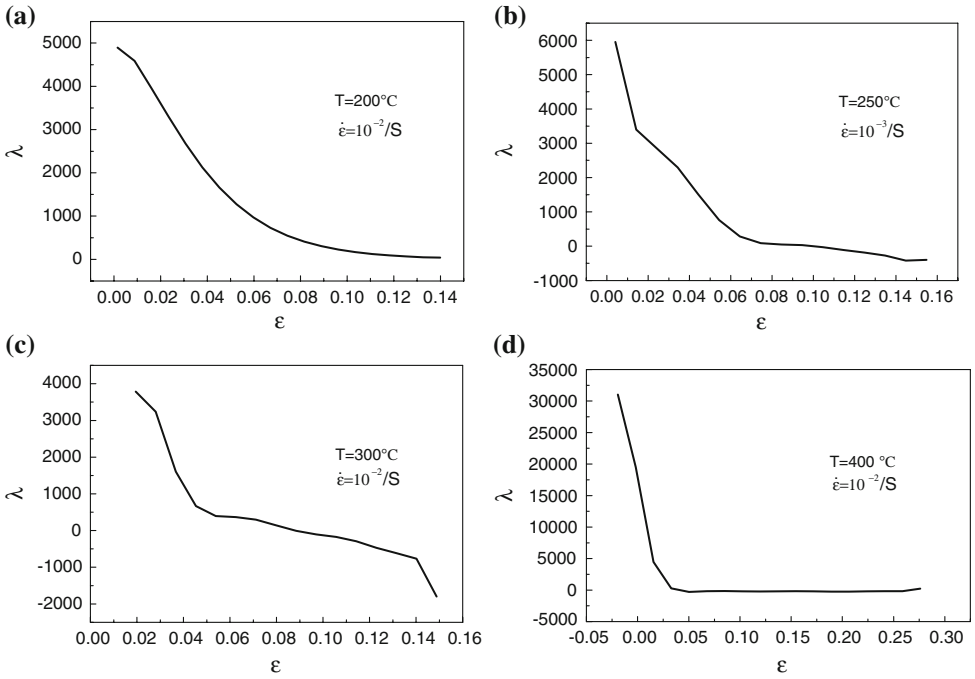

Fig. 4 Curves of λ as a function of ε: **a** 200 °C, $\dot{\varepsilon} = 10^{-2}\,s^{-1}$; **b** 250 °C $\dot{\varepsilon} = 10^{-3}\,s^{-1}$; **c** 300 °C, $\dot{\varepsilon} = 10^{-2}\,s^{-1}$; and **d** 400 °C $\dot{\varepsilon} = 10^{-2}\,s^{-1}$

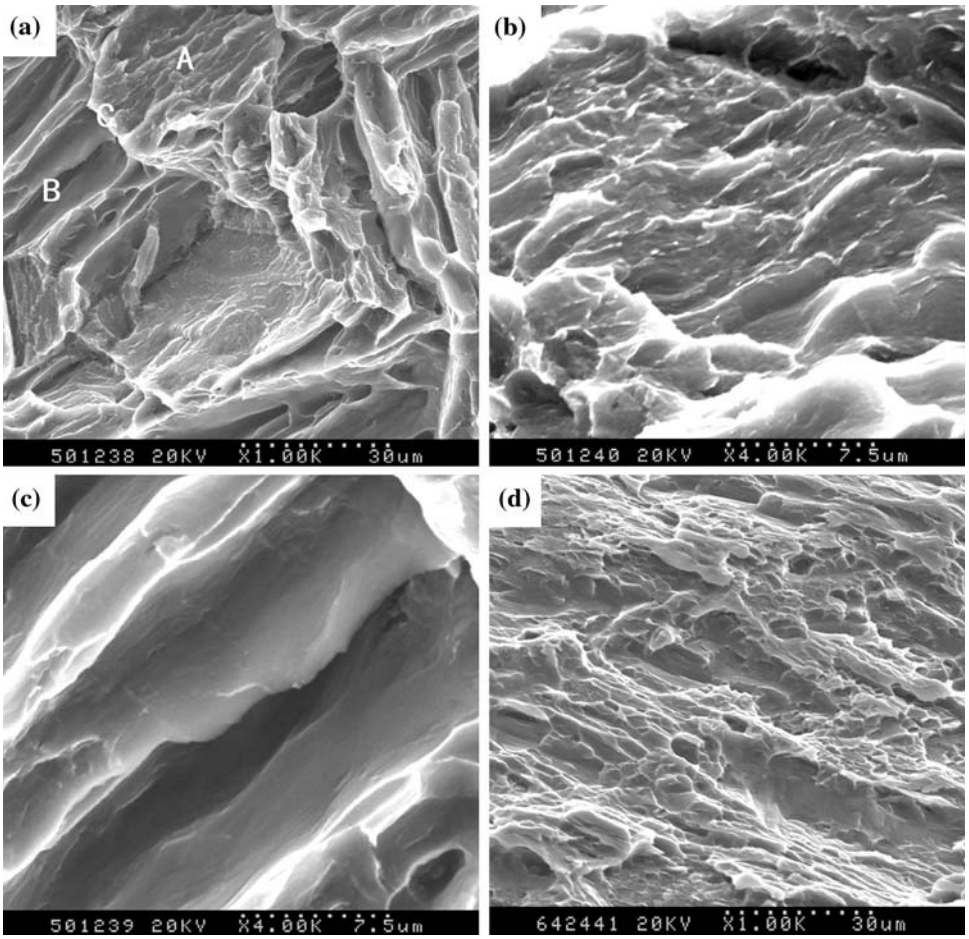

Fig. 5 Tensile fractgraphies of Mg–Nd–Zn–Zr alloy tested at 100 °C and $\dot{\varepsilon} = 10^{-4}\,s^{-1}$. **a** Center; **b** enlargement of A in **a**; **c** enlargement of B in **a**; and **d** edge

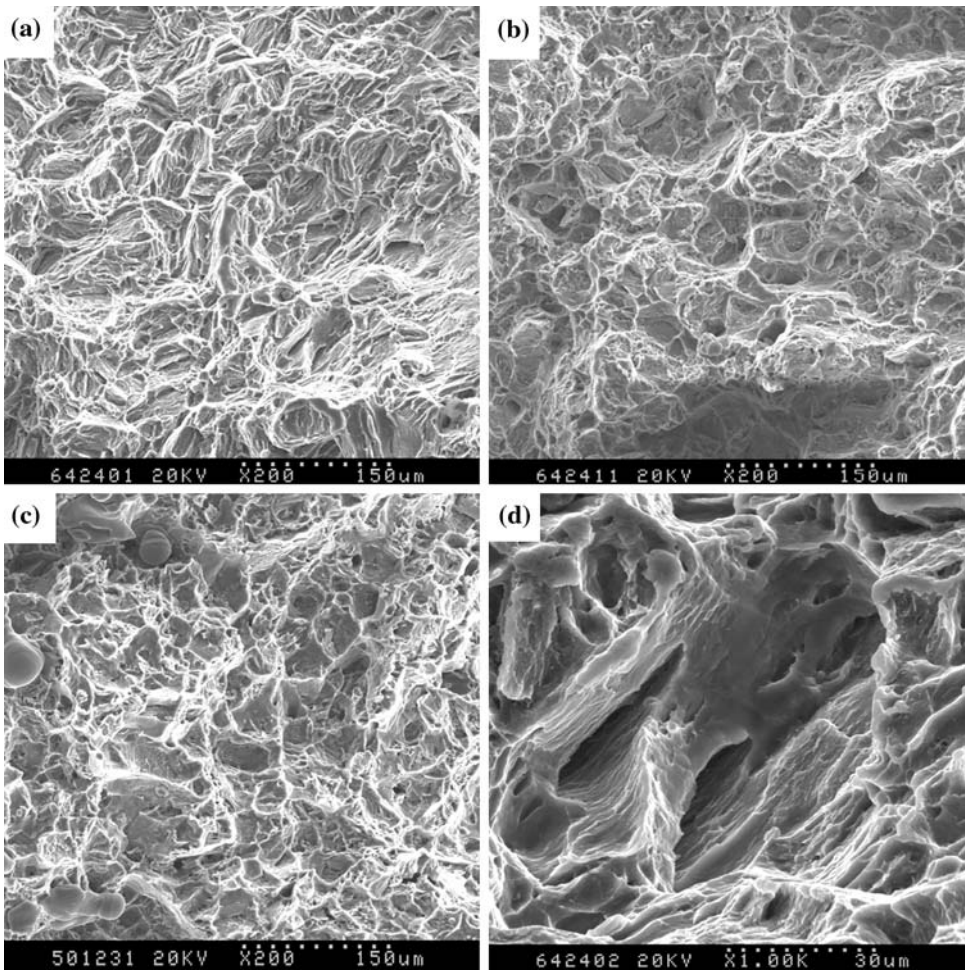

Fig. 6 Tensile fractgraphies of Mg–Nd–Zn–Zr alloy tested at 250 °C. **a** $\dot{\varepsilon} = 10^{-2}\,s^{-1}$, **b** $\dot{\varepsilon} = 10^{-3}\,s^{-1}$, **c** $\dot{\varepsilon} = 10^{-4}\,s^{-1}$, and **d** crack in dimple

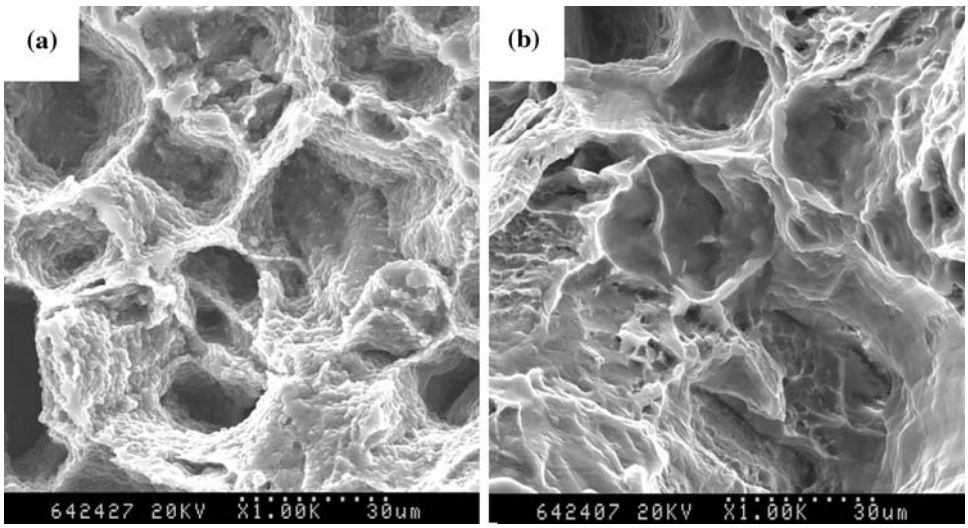

Fig. 7 Fractgraphies of Mg–Nd–Zn–Zr alloy at elevated temperature. **a** $\dot{\varepsilon} = 10^{-4}\,s^{-1}$, 300 °C, and **b** $\dot{\varepsilon} = 10^{-2}\,s^{-1}$, 400 °C

in Fig. 4d falls down to zero abruptly at a very small engineering strain of 0.05 and keeps constant subsequently, indicating that the decrease in engineering stress has a linear relationship with the increase in engineering strain during necking.

Fracture analysis

The tensile fractographs tested at 100 °C with strain rate of $10^{-4}\,s^{-1}$ are shown in Fig. 5. Point A refers to herring-bone-like cleavages and Point B is river pattern crack, and

Point C is boundary in Fig. 5a. Figure 5b and c are the enlargements of Point A and B in Fig. 5a, respectively. Additionally, there are a small amount of elongated dimples and trace of intergranular crack existing at the edge of fracture. The fracture mode is cleavage fracture mainly accompanied with a small amount of elongated dimples at 100 °C and strain rate has little effect on the fractography.

The tensile fractographs tested at 250 °C with strain rates of 10^{-4} s^{-1}, 10^{-3} s^{-1}, and 10^{-2} s^{-1} are shown in Fig. 6. There are two typical kinds of dimples, round and flat. For the highest strain rate used in present study of 10^{-2} s^{-1}, flat dimples are the majority and both are much shallow and non-uniformly distributed as shown in Fig. 6a. With decreasing strain rate, the flat dimples deplete gradually and the round ones become major as shown in Fig. 6b and c, indicating that the type of dimple is strongly dependent on strain rate at 250 °C. There are new cracks forming at the big dimple wall, which initiate new dimples as shown in Fig. 6d. The transition of fracture mechanism is likely the fact which attributes to the increasing of engineering stress caused by the medium strain rate in Fig. 1b. The fractographs at 300 °C with strain rate of 10^{-4} s^{-1} and at 400 °C with 10^{-2} s^{-1} are given in Fig. 7. They are typically dimple fractures and similar with each other. The deep dentritic dimple distributes uniformly on the fracture surface, which are benefit for plasticity increase. The difference between Fig. 7a and b is that there is oxidation film on the fractured surface due to the long deformation time near 1 h caused by low strain rate at relatively high temperature. It is unavoidable for fracture surface to oxide due to the high affinity of Mg to oxygen even under the protection of vacuum of 0.6 Pa, resulting in surface degradation [11]. The dimple wall is rugous and consists of tiny particles deposited. Although the latter is tested at much high temperature of 400 °C, no obvious oxide film existing because of a short deformation time of less than 10 s and the dimple wall is smooth.

Conclusions

The tensile deformation behaviors of a heat treated Mg–Nd–Zn–Zr alloy at elevated temperature up to 400 °C were investigated systematically. Below 250 °C, the engineering stress quickly reaches a peak at very low engineering strain, followed by a gradual increase until failure. Strain rate has little effect on engineering stress and the fracture characterization is typical brittle. At 250 °C, there is transition existing from flat dimple to round one as strain rate decreases from 10^{-2} s^{-1} to 10^{-4} s^{-1}. Above 300 °C, the fracture is of typical ductile failure and higher temperature results in dramatic decrease in engineering stress and the effect of strain rate is significant.

References

1. Sanchez C, Nussbaum G, Azavant P, Octor H (1996) Mater Sci Eng A221:48
2. Nie JF, Muddle BC (2000) Acta Mater 48:1691
3. Chino Y, Kad M, Mabuchi M (2008) Acta Mater 56:387
4. Somekawa H, Mukai T (2007) Mater Sci Eng A459:366
5. Qian M, St John DH, Frost MT (2003) In: Kainer KU (ed) Magnesium alloys and their applications. Wiley-VCH, Weinheim, pp 706–712
6. Kettner M, Noster U, Kilian H, Gradinger R, Kuhlein W (2006) In: Kainer KU (ed) Magnesium alloys and their applications. Wiley-VCH, Weinheim, pp 305–317
7. St John DH (2007) Mater Sci Forum 546–549:49
8. Zhilliang N, Haibo W, Weizhong L et al (2004) J Chin Rare Earth Soc 22(1):134
9. Zhiliang N, Fuyang C, Jianfei S, Jianfeng D (in press) Mater Eng
10. Changqing X, Wenhua W, Anru W, Yinn W (2004) Chin J Nonferrous Met 14(11):1810
11. Ning Z, Liang W, Cao F, Sun J (2009) Int J Mod Phys B 23(6–7): 796